Journal of Optics

OPEN ACCESS

RECEIVED
23 December 2025

REVISED
15 February 2026

ACCEPTED FOR PUBLICATION
6 March 2026

PUBLISHED
19 March 2026

PAPER

Analysis of pulse compression in a high repetition rate and high average power Yb-fiber based hybrid PCMA-FCPA femtosecond laser system

Jokūbas Pimpė[1,2,*], **Vygandas Jarutis**[1] and **Julius Vengelis**[1]

[1] Vilnius University Laser Research Center, Saulėtekio Ave. 10, Vilnius LT-10223, Lithuania
[2] Light Conversion Ltd., Keramiku str. 2B, Vilnius LT-10232, Lithuania
[*] Author to whom any correspondence should be addressed.

E-mail: jokubas.pimpe@ff.vu.lt

Keywords: FCPA, PCMA, high average power femtosecond pulses, high repetition rate femtosecond pulses, Yb-doped fiber amplifier

Abstract

We present a comprehensive experimental and theoretical analysis of high repetition rate and high average power femtosecond pulse amplification and temporal compression in a hybrid pre-chirp managed amplification (PCMA) and fiber chirped pulse amplification (FCPA) system. We investigate the influence of initial pulse chirp, gain dynamics and nonlinear self-phase modulation on the temporal and spectral characteristics of amplified pulses. Numerical simulation results agreed well with experiments and demonstrated that improper selection of the input chirp at a constant amplified pulse output power can lead to poor pulse compression quality. Our analysis explains the relation between pre-chirp and output pulse compressibility and provides important insights into optimizing hybrid PCMA–FCPA systems for generating high average power and high repetition rate femtosecond laser systems with nearly transform-limited pulse durations.

1. Introduction

The demand for high average power (>50 W), high repetition rate (tens of MHz) femtosecond laser systems [1] continues to rise due to their unique features, such as the ability to decrease experimental data acquisition time and enable higher signal-to-noise ratio [2], which is highly applicable in various fields ranging from precision micromachining [3] to nonlinear optics [4], lithography [5], microscopy [6] and high-field physics [7]. Simultaneously achieving high average power, short pulse duration and excellent beam quality at tens of MHz repetition rates requires careful management of thermal load, gain dynamics, nonlinear effects and long-term stability [8]. Yb-doped fiber amplifiers are particularly attractive for such systems due to their efficient heat dissipation, large surface-to-volume ratio, and excellent beam quality [9–11]. Despite their superiority, fiber-based systems face challenges arising from nonlinear optical effects, transverse mode instabilities and material damage [12–14]. Large-mode-area (LMA) double-clad photonic crystal fibers (PCFs) mitigate nonlinear effects by increasing the effective mode area while maintaining high pump absorption and near-diffraction-limited beam quality [15–17]. In parallel, chirped-pulse amplification remains the standard approach for reducing nonlinearities in Yb-fiber systems [18]. However, limitations in pulse stretching to nanoseconds, gain narrowing and residual dispersion mismatch, typically limit the compressed pulse duration to several hundreds of femtoseconds [19, 20]. Therefore, nonlinear amplification regimes such as self-similar (parabolic) pulse amplification [21, 22], pre-chirp managed amplification (PCMA) [23, 24] or gain managed amplification [25] have been developed to overcome these constraints. These techniques deliberately exploit the interplay between self-phase modulation (SPM) and normal dispersion to broaden the optical spectrum during amplification, thus enabling the generation of sub-100 fs pulses [9, 26]. While PCMA provides strong spectral broadening, residual temporal pedestals may appear, whereas conventional linear fiber chirped pulse amplification (FCPA) stages are constrained by gain bandwidth [27, 28]. Combining the two approaches in a hybrid PCMA–FCPA architecture leverages the advantages of both regimes: the stability and power scalability of FCPA, combined with the spectral broadening and compressibility of PCMA

[29]. However, experimental studies repeatedly observe that pulses amplified in hybrid PCMA–FCPA systems can fail to compress amplified pulses with certain values of pre-chirp, even when output power and spectral width appear favorable [19, 23, 29]. Although most current numerical models aim to improve compressed pulse quality by optimizing input parameters such as pre-chirp, gain, and power, they rarely address the underlying physical mechanisms responsible for poor pulse compressibility [26, 27, 30]. As a result, the origin of the experimentally observed 'incompressible chirp regions' remains unclear.

In this work, we investigate this effect by performing a comprehensive numerical study of pulse amplification and compression in our recently demonstrated hybrid PCMA–FCPA Yb-doped rod-type PCF amplifier. By coupling a time-dependent rate-equation model for gain dynamics with the generalized nonlinear Schrödinger equation, we examine the influence of input chirp, fiber nonlinearity and gain dynamics on spectral evolution and pulse compressibility in detail. We show and explain why inappropriate selection of input chirp can strongly degrade compression quality even at constant output power. The results provide practical guidelines for optimizing configuration of hybrid fiber amplifiers capable of generating high power, high repetition rate and nearly transform-limited (TL) femtosecond pulses.

2. Experimental setup

Figure 1 illustrates the configuration of the hybrid PCMA–FCPA amplification system we built and analyzed [29]. The seed source was a commercial Kerr-lens mode-locked Yb:KGW oscillator (FLINT, Light Conversion) operating at 76 MHz repetition rate and with an average output power of 6 W. The central wavelength of the femtosecond pulses was around 1028 nm with 15.5 nm spectral bandwidth (FWHM) and slightly chirped pulse duration of 112 fs (compressible to 98 fs). Temporal stretching of the oscillator pulses was achieved using a four-pass transmission-grating stretcher G1 (800 lines mm^{-1}, 97% first-order diffraction efficiency, Wasatch Photonics). The degree of stretching was controlled by adjusting the spacing between G1 and a $f = +150$ mm focal length lens (L1). This configuration allowed the group delay dispersion (GDD) to vary between 0.024 ps^2 and 2.47 ps^2, enabling stretched pulse durations from 600 fs to 60 ps. The seed power after pulse stretching was 5.2 W, corresponding to pulse energy of approximately 68 nJ. Pulse amplification was performed in a 80.4 cm length polarization-maintaining, double-clad, LMA PCF (aeroGAIN-ROD-PM85, NKT Photonics) with an 85 μm core and 260 μm cladding diameters. Both fiber ends were equipped with anti-reflection coated end caps and the fiber was water-cooled to ensure stable thermal operation. The seed pulse was guided towards the fiber input using dielectric mirror M and a dichroic mirror DM1 (highly reflective at 1030 nm and transmissive at 976 nm) and coupled into the fiber's core with a $f = +60$ mm lens (L2), which matched the seed beam width to the fiber core mode size. The dichroic mirror DM1 was also used to transmit the residual

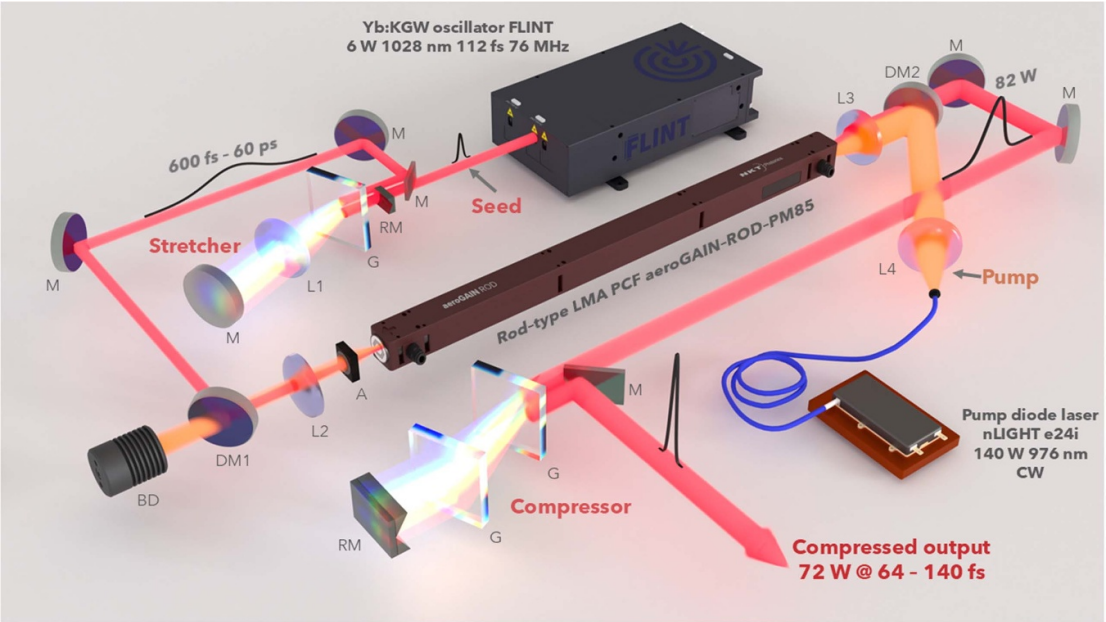

Figure 1. Schematic layout of the PCMA-FCPA amplification system. G1, G2 and G3, transmission diffraction gratings; L1, L2, L3, L4, lenses; M, high reflection beam steering mirrors; DM1, DM2, dichroic mirrors; RM, retroreflector; A, water-cooled aperture; BD, beam dump. Reprinted from [29], Copyright (2025), with permission from Elsevier.

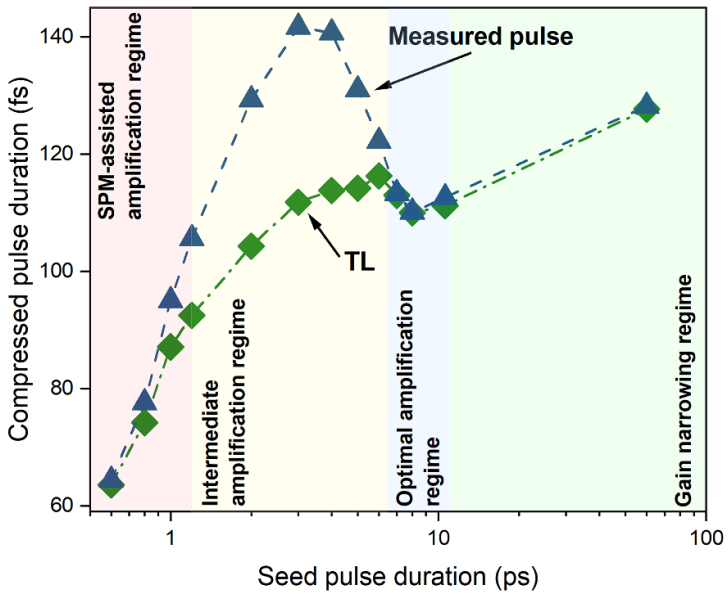

Figure 2. The experimentally measured compressed pulse durations (blue) and their corresponding transform-limited (TL) pulse durations (green) as a function of the seed pulse duration. The shaded areas indicate different PCMA-FCPA amplifier system operating regimes. Reprinted from [29], Copyright (2025), with permission from Elsevier.

pump light toward a beam dump, while a water-cooled aperture (A) blocked residual pump radiation, preventing additional thermal load onto the steering optical mounts. To preserve the input seed pulse polarization, a half-wave plate was placed before DM1 to adjust the seed's polarization in respect to the slow or fast axis of the fiber. The amplifier was pumped by a continuous-wave 976 nm diode laser (e24i, nLIGHT) delivering up to 140 W of output power. The pump beam was coupled into the fiber using a steering dichroic mirror DM2 (with high reflectivity at 976 nm and high transmission at 1030 nm) and numerical aperture matching lens set—L3 ($f = +20$ mm) and L4 ($f = +30$ mm). LMA PCF featured an exceptional power handling with a 3300 μm^2 mode area and mode field diameter of 65 μm $\pm$ 5 μm (as specified by the producer) and high pump absorption of >15 dB over the entire fiber length. The amplified output pulse beam was collimated using the same aspheric lens L3 and guided towards a double-pass pulse compressor. Compression was performed using a pair of transmission diffraction gratings (G2 and G3) identical to G1, along with a retroreflector mirror (RM), allowing to compensate GDD up to the third order with total transmission of approximately 88%. The amplified output pulse temporal characteristics were analyzed by using an in-house second-harmonic generation frequency-resolved optical gating system equipped with a 50 μm-thick beta-barium borate crystal and using a standard retrieval algorithm for trace reconstruction, while spectral characteristics were registered with a spectrometer (Avaspec-2048-SPU, Avantes). When fully optimized, the system delivers 114 fs pulses with 72 W average power at 76 MHz repetition rate centered at 1032 nm wavelength, beam quality of $M^2 < 1.1$ and long-term stability of 0.2% (RSD).

The comparison between experimentally measured pulse durations and the TL pulse widths, estimated from the zero-phase Fourier transform of the measured spectra, is summarized in figure 2. We distinguished several distinct operating regimes of PCMA-FCPA laser system according to the seed pulse duration, with the most interesting being the 'intermediate amplification regime', which corresponds to seed pre-chirp pulse durations in the range of 1.2–6 ps. In this region, we observe the largest and most significant mismatch between the measured compressed pulse duration and the TL value, with the maximum discrepancy reaching almost 30 fs at a 3 ps pre-chirp. In contrast, the surrounding regions, such as the 'SPM-assisted amplification regime', which yields the shortest pulse durations but with horn-shaped spectra, and the 'optimal amplification region', where temporal and spectral distortions are minimal, thus produces pulses with characteristics similar to the initial seed, which are not affected by the gain-narrowing effect, as observed in the last operating regime.

3. Numerical simulation of pulse compression in a hybrid FCPA-PCMA system

3.1. Initial pulse

In our model, pulse chirping and compression are performed by adding or removing the quadratic phase of the spectrum. Although in reality any spectrum-modifying device also affects the higher-order

spectral phase, this approximation is sufficient to reproduce the results observed in the experiment. So, here we assume that at the input of the amplifier we have a chirped Gaussian pulse

$$A(t) = \frac{A_0}{\sqrt{1+\mathrm{i}\gamma}} \mathrm{e}^{-\frac{t^2}{\tau_0^2(1+\mathrm{i}\gamma)}}, \tag{1}$$

where $\tau_0 = 2/\Delta\Omega_{1/e^2}$ is the characteristic pulse duration defined uniquely by the width of the initial pulse spectra $\Delta\Omega_{1/e^2}$ at the $1/e^2$ level of the spectral intensity and γ is the dimensionless chirp parameter, which is related to the GDD as $\gamma = 2\,\mathrm{GDD}/\tau_0^2$.

3.2. Preliminary analysis

To explain the results observed in the experiment, it is useful to discuss an analytically solvable model, i.e the propagation of a chirped pulse in a dispersionless medium with Kerr-type nonlinearity. In the simplest case, the model equation is as follows

$$\frac{\partial A}{\partial z} = -\mathrm{i}\sigma|A|^2 A, \tag{2}$$

where σ is a nonlinear coefficient of self phase modulation (SPM) for a pulse central frequency ω_0 and A is a slowly varying complex amplitude of the pulse. If we assume that at the input there is a chirped pulse with complex amplitude given by the equation (1), then the amplitude of the pulse at the output ($z > 0$) is $A_{\mathrm{out}} = |A_{\mathrm{in}}|\exp(\mathrm{i}\phi)$, with the phase

$$\phi = \frac{\gamma t^2}{\tau^2} - \sigma z|A_{\mathrm{in}}|^2 - \frac{1}{2}\arctan\gamma, \tag{3}$$

and $\tau = \tau_0\sqrt{(1+\gamma^2)}$. A simple way to quantify the compressibility of the pulse is to calculate the covariation between the instantaneous frequency and the time of the pulse

$$\mathrm{Cov}_{t,\omega_i} = \int_{-\infty}^{\infty} t\omega_i|A_{\mathrm{out}}|^2\mathrm{d}t \Big/ \int_{-\infty}^{\infty}|A_{\mathrm{out}}|^2\mathrm{d}t\,. \tag{4}$$

The larger the covariance, the closer is the instantaneous frequency variation vs time to a linear variation on average and the better the output pulse can be compressed. In this case, the instantaneous frequency is

$$\omega_i = \omega_0 + \frac{\mathrm{d}\phi}{\mathrm{d}t} = \omega_0 + \frac{2t}{\tau^2}\left(\gamma + 2\sigma z|A_{\mathrm{in}}|^2\right), \tag{5}$$

and the covariance is

$$\mathrm{Cov}_{t,\omega_i} = \frac{1}{2}\left(\gamma + \frac{\sigma|A_0|^2 z}{\sqrt{2(1+\gamma^2)}}\right) \underset{\gamma>5}{\approx} \frac{1}{2}\left(\gamma + \frac{\sigma|A_0|^2 z}{\sqrt{2}\gamma}\right). \tag{6}$$

The covariance expression definitely has the minimum when $\gamma \approx (\sigma|A_0|^2 z/\sqrt{2})^{1/2}$, which means that for this chirp value the compression of the output pulse is the worst. Although this simple analysis is not directly applicable to a real experiment, as it does not take into account other phenomena such as pulse amplification, material dispersion, and nonlinear pulse group velocity dispersion (GVD), it is still instructive, as it indirectly demonstrates the possibility of obtaining poorly compressed pulses. A more detailed and accurate analysis of the experiment can only be performed by taking into account all the aforementioned phenomena and solving the problem numerically.

3.3. Signal pulse amplification

The amplification of the signal pulse takes place in the fiber core doped with Yb atoms, which are excited by continuous-wave radiation of wavelength $\lambda_{\mathrm{p}} = 976$ nm, see figure 3. In the two-level atom model, N_1 is the fraction of Yb atoms that are in the ground state, and N_2 is the fraction of excited atoms. In the absence of a signal pulse, the fractional concentrations N_1 and N_2 depend only on the pump beam, and their evolution is described by equations [31]

$$\frac{\partial N_2}{\partial t} = \left[\sigma_{12}(\nu_{\mathrm{p}})N_1 - \sigma_{21}(\nu_{\mathrm{p}})N_2\right]\frac{I_{\mathrm{p}}}{h\nu_{\mathrm{p}}} - \frac{N_2}{T}, \tag{7}$$

$$N_1 = 1 - N_2, \tag{8}$$

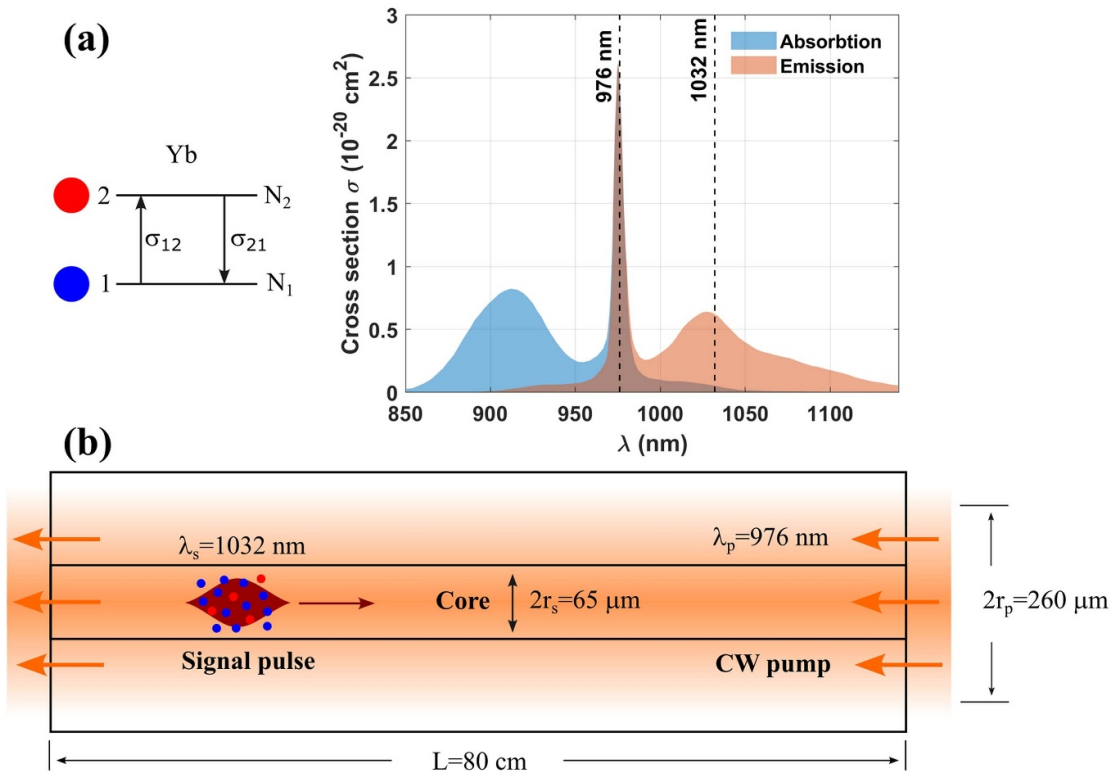

Figure 3. (a)—The pulse amplification takes place in a Yb-doped polarization-maintaining double-clad rod. The Yb atoms are excited by continuous-wave 976 nm radiation. The spectral amplification efficiency depends on the concentration of excited (N_2) and ground-state (N_1) Yb atoms under the pulse envelope, as well as on the absorption (σ_{12}) and emission (σ_{21}) cross section coefficients based on data reported in [31]. (b)—The signal pulse propagates in the inner fiber core in the opposite direction to the CW radiation and interacts with the Yb atoms.

$$\frac{\partial I_\mathrm{p}}{\partial z} = \left[\sigma_{21}(\nu_\mathrm{p})N_2 - \sigma_{12}(\nu_\mathrm{p})N_1\right] N_\mathrm{a} I_\mathrm{p}\,, \tag{9}$$

where $\sigma_{12}\nu_\mathrm{p})$ and $\sigma_{21}\nu_\mathrm{p})$ are the absorption and emission cross section coefficients of the Yb atom respectively for the frequency ν_p, T is the spontaneous relaxation time of the excited atom and N_a is the concentration of Yb atoms. The signal pulse, propagating through the medium, finds a steady state equilibrium between the Yb atoms and the CW pump radiation. The concentrations of the corresponding atoms are then found from the condition $\partial_t N_2 = 0$, i.e.

$$N_{20}(z) = \mathcal{N}\frac{I_\mathrm{p}(z)}{I_\mathrm{p}(z) + I_\mathrm{ps}}\,, \tag{10}$$

$$N_{10}(z) = 1 - N_{20}(z)\,. \tag{11}$$

Here, $\mathcal{N}$ stands for the maximum concentration of excited atoms

$$\mathcal{N} = \frac{\sigma_{12}(\nu_\mathrm{p})}{\sigma_{12}(\nu_\mathrm{p}) + \sigma_{21}(\nu_\mathrm{p})}\,, \tag{12}$$

formally reached only when $I_\mathrm{p} \to \infty$, I_ps—pump saturation intensity

$$I_\mathrm{ps} = \frac{h\nu_\mathrm{p}}{T(\sigma_{12}(\nu_\mathrm{p}) + \sigma_{21}(\nu_\mathrm{p}))}\,, \tag{13}$$

at which half of the theoretically possible Yb atoms are excited, i.e. $N_{20} = \mathcal{N}/2$. The pump beam intensity distribution $I_\mathrm{p}(z)$ along the fiber at equilibrium is found by solving equation (9) substituting $N_1 = N_{10}z)$ and $N_2 = N_{20}z)$. From this we find that $I_\mathrm{p}(z)$ satisfies the algebraic equation

$$I_\mathrm{p}\,(z)\exp\left(\frac{I_\mathrm{p}\,(z)}{I_\mathrm{ps}}\right) = I_{\mathrm{p}0}\exp\left(\frac{I_{\mathrm{p}0}}{I_\mathrm{ps}} - \Gamma_\mathrm{p} z\right)\,, \tag{14}$$

Table 1. The parameter values used in the equation (20) to estimate the change in the concentration of excited Yb atoms due to the interaction with the signal pulse.

Pump parameters	
Central wavelength	$\lambda_p = 976\,\text{nm}$
Average power	$P_p = 140\,\text{W}$
Diameter of the beam at FWHM	$2r_p = 260\,\mu\text{m}$
Peak intensity	$I_p = 1.83 \times 10^5\,\text{W cm}^{-2}$
Absorption cross section	$\sigma_{12}^{(p)} = 2.4854 \times 10^{-20}\,\text{cm}^2$
Emission cross section	$\sigma_{21}^{(p)} = 2.4854 \times 10^{-20}\,\text{cm}^2$
Signal parameters	
Central wavelength	$\lambda_s = 1032\,\text{nm}$
Diameter of the beam at FWHM	$2r_s = 65\,\mu\text{m}$
Pulse repetition rate	$\nu_L = 76\,\text{MHz}$
Average power	$5 < P_s < 80\,\text{W}$
Pulse duration	$1 < \tau_s < 100\,\text{ps}$
Peak intensity	$0.04 < I_s < 60\,\text{GW cm}^{-2}$
Absorption cross section	$\sigma_{12}^{(s)} = 5.32 \times 10^{-22}\,\text{cm}^2$
Emission cross section	$\sigma_{21}^{(s)} = 62.3 \times 10^{-22}\,\text{cm}^2$

where $\Gamma_p = \sigma_{12}\nu_p)N_a$ is the absorption coefficient and I_{p0} is the intensity of the pump beam at the entrance of the amplifier.

Next, we estimate how much the signal pulse itself changes the concentration of excited Yb atoms. To this end, we supplement the equation (7) by including the signal

$$\frac{\partial N_2}{\partial t} = \left[\sigma_{12}^{(p)} N_1 - \sigma_{21}^{(p)} N_2\right] \frac{I_p}{h\nu_p} - \frac{N_2}{T} + \left[\sigma_{12}^{(s)} N_1 - \sigma_{21}^{(s)} N_2\right] \frac{I_s}{h\nu_s}. \tag{15}$$

Setting $N_2 = N_{20} + \delta N_2$, $N_1 = N_{10} + \delta N_1$ and taking into account that $\delta N_1 = -\delta N_2$, we obtain the equation for the evolution of the excited Yb atom concentration deviation δN_2 from equilibrium N_{20}

$$\frac{\partial\, \delta N_2}{\partial t} = -\frac{\delta N_2}{T_s} + R_s. \tag{16}$$

where

$$\frac{1}{T_s} = \left(\sigma_{12}^{(p)} + \sigma_{21}^{(p)}\right) \frac{I_p}{h\nu_p} + \frac{1}{T} + \left(\sigma_{12}^{(s)} + \sigma_{21}^{(s)}\right) \frac{I_s}{h\nu_s}, \tag{17}$$

$$R_s = \left[\sigma_{12}^{(s)} N_{10} - \sigma_{21}^{(s)} N_{20}\right] \frac{I_s}{h\nu_s}. \tag{18}$$

Taking into account the initial condition $\delta N_2(0) = 0$ we find that the solution of equation (16) is

$$\delta N_2\,(t) = T_s R_s \left(1 - \mathrm{e}^{-t/T_s}\right). \tag{19}$$

The largest relative change in the concentration of excited atoms in terms of magnitude is

$$\epsilon = \frac{\delta N_2}{N_{20}} = \frac{T_s R_s}{N_{20}}. \tag{20}$$

For spontaneous relaxation time $T = 1.5\,\text{ms}$, Yb atom concentration $N_a = 10^{19}\,\text{cm}^{-3}$ and other parameters listed in table 1, we obtain $\epsilon = -6 \times 10^{-4}$. In other words, the amplification of the signal pulse occurs gradually and the change in the concentration of excited Yb atoms under the pulse envelope is insignificant, so we may assume that $N_2 \approx N_{20}z)$. This allows us to define the gain coefficient for the signal pulse as

$$g(z,\omega) = \frac{1}{2}\left(\sigma_{21}(\omega) N_{20}(z) - \sigma_{12}(\omega) N_{10}(z)\right) N_a. \tag{21}$$

3.4. Self-modulation of signal pulse

In an isotropic medium, the lowest order nonlinear polarization can be expressed as follows

$$P_n(t) = \varepsilon_0 \int \mathrm{d}\boldsymbol{\tau}\, R(\boldsymbol{\tau})\, E(t-\tau_1)\, E(t-\tau_2)\, E(t-\tau_3)\,, \tag{22}$$

where $R(\boldsymbol{\tau}) = R(\tau_1, \tau_2, \tau_3)$ is a nonlinear response function, E is an electric field, and $\int \mathrm{d}\boldsymbol{\tau}$ stands for $\iiint \mathrm{d}\tau_1 \mathrm{d}\tau_2 \mathrm{d}\tau_3$ with integration limits of 0 to ∞. Expressing the electric field in terms of the amplitude of the pulse envelope $\mathcal{E}$

$$E(t) = \mathrm{e}^{\mathrm{i}\omega_0 t - \mathrm{i}k_{0z}}\, \mathcal{E}t) + \mathrm{c.c.}\,, \tag{23}$$

and considering only the nonlinear polarization responsible for SPM, we obtain

$$\mathcal{P}_{\mathrm{SPM}}(t) = 3\varepsilon_0 \int \mathrm{d}\boldsymbol{\tau}\, R(\boldsymbol{\tau})\, \mathrm{e}^{\mathrm{i}\omega_0 \Delta\tau} \mathcal{E}(t-\tau_1)\mathcal{E}(t-\tau_2)\mathcal{E}^*(t-\tau_3)\,, \tag{24}$$

where $\Delta\tau = \tau_3 - \tau_2 - \tau_1$. The electronic or Kerr response is often imagined as instantaneous. Here we follow a more general approach, i.e. we assume that the electronic response occurs over a finite time, which is much shorter than the pulse duration. In this case, expanding the envelope amplitudes of the pulse in a series with respect to τ_1, τ_2 and τ_3 and discarding small quantities of order higher than the first, we obtain the following result

$$\mathcal{P}_{\mathrm{SPM}}(t) = 3\varepsilon_0 \left(\chi \mathcal{E}|\mathcal{E}|^2 - 2\alpha_{1,2} \frac{\partial \mathcal{E}}{\partial t} |\mathcal{E}|^2 - \alpha_3 \mathcal{E}^2 \frac{\partial \mathcal{E}^*}{\partial t} \right), \tag{25}$$

where we denote

$$\chi \equiv \int \mathrm{d}\boldsymbol{\tau}\, R(\boldsymbol{\tau})\, \mathrm{e}^{\mathrm{i}\omega_0 \Delta\tau}\,, \tag{26}$$

$$\alpha_{1,2} \equiv \int \mathrm{d}\boldsymbol{\tau}\, R(\boldsymbol{\tau}) \cdot \tau_{1,2}\, \mathrm{e}^{\mathrm{i}\omega_0 \Delta\tau}\,, \tag{27}$$

$$\alpha_3 \equiv \int \mathrm{d}\boldsymbol{\tau}\, R(\boldsymbol{\tau}) \cdot \tau_3 \mathrm{e}^{\mathrm{i}\omega_0 \Delta\tau}\,. \tag{28}$$

From the definitions it follows that the coefficients $\alpha_{1,2}$, α_3 satisfy the relation

$$\alpha_3 - 2\alpha_{1,2} = -\mathrm{i}\frac{\partial \chi}{\partial \omega_0}\,. \tag{29}$$

It is obvious that $\chi' \equiv \partial\chi/\partial\omega_0$ describes the dispersion of nonlinear dielectric susceptibility χ due to the change of the central frequency of the pulse. Equation (29) will always be satisfied if, instead of the coefficients $\alpha_{1,2}$, α_3 we rewrite them as follows

$$\alpha_{1,2} = \mathrm{i}\chi' + \mathrm{i}\frac{\beta}{2}\,, \tag{30}$$

$$\alpha_3 = \mathrm{i}\chi' + \mathrm{i}\beta\,. \tag{31}$$

The nonlinear polarization responsible for the self-modulation can then be rewritten as

$$\mathcal{P}_{\mathrm{SPM}}(t) = 3\varepsilon_0 \left(\chi \mathcal{E}|\mathcal{E}|^2 - \mathrm{i}\chi' \frac{\partial}{\partial t}\left(\mathcal{E}|\mathcal{E}|^2\right) - \mathrm{i}\beta \mathcal{E} \frac{\partial |\mathcal{E}|^2}{\partial t} \right). \tag{32}$$

The coefficient β describes the change in the group velocity of a pulse due to nonlinear self-modulation and, at the same time, affects the dispersion of the nonlinear dielectric susceptibility. To make the expressions clearer, we write χ' and β in terms of dielectric susceptibility χ as $\chi' = \chi\tau_{\mathrm{K}}$ and $\beta = \chi\tau_G$. The characteristic duration τ_{K} can be interpreted as the duration of the Kerr temporal response, and τ_{G} is a nonlinear delay due to self modulation. Calculating the Fourier transforms of both sides of (32), we find

$$\hat{\mathcal{P}}_{\mathrm{SPM}}\Omega) = 3\varepsilon_0\chi \left((1 + \tau_{\mathrm{K}}\Omega)\, \mathcal{F}\left\{\mathcal{E}|\mathcal{E}|^2\right\} - \mathrm{i}\tau_{\mathrm{G}} \mathcal{F}\left\{ \mathcal{E}\frac{\partial |\mathcal{E}|^2}{\partial t} \right\} \right), \tag{33}$$

where $\mathcal{F}$ denotes the Fourier transform.

3.5. Model equation

The simulation of pulse propagation is performed in a moving coordinate system $z' = z$, $t' = t - k_0' z$, where $k_0' = (\mathrm{d}k/\mathrm{d}\omega)_{\omega_0}$ and $1/k_0' = v$ is the group velocity of the pulse. The complex amplitude of the impulse in the moving coordinate system is $A(z', t') = \mathcal{E}z', t' + k_0' z')$. To simplify the expressions, we rename $t' \to t$ and $z' \to z$. Taking into account the signal pulse amplification, dispersion, and Kerr-like self-modulation, the evolution of the signal spectrum in the amplifier, using the slowly varying amplitude method, is described by the equation

$$\frac{\partial \hat{S}}{\partial z} = \hat{g}\hat{S} - \mathrm{i}k_\mathrm{D}\hat{S} - \mathrm{i}k_\mathrm{N}\left((1+\tau_\mathrm{K}\Omega)\,\mathcal{F}\left\{\hat{A}|\hat{A}|^2\right\} - \mathrm{i}\tau_\mathrm{G}\,\mathcal{F}\left\{\hat{A}\frac{\partial|\hat{A}|^2}{\partial\hat{t}}\right\}\right), \tag{34}$$

where $\hat{A} = A/A_0$ is the dimensionless amplitude of the pulse, $\hat{S} = \mathcal{F}\{\hat{A}\}$ is the spectrum. The gain coefficient $\hat{g} = g(L-z,\omega)$ takes into account that the CW pump and signal pulse propagate in opposite directions. The linear dispersion coefficient is $k_\mathrm{D} = k - \kappa$, $\kappa = k_0 + k_0'\Omega$, $k_0 = k(\omega_0)$ is the wavenumber corresponding to the central signal frequency ω_0, and $\Omega = \omega - \omega_0$. The self-modulation of a signal pulse is described by the nonlinear wave number

$$k_\mathrm{N}(\Omega) = \frac{2n_0 n_2 I_0}{k+\kappa}\,\frac{\omega^2}{c^2}, \tag{35}$$

where $n_2 = 3\chi/(4\varepsilon_0 c n_0^2) = 2.6\times10^{-16}\,\mathrm{cm}^{-2}\,\mathrm{W}$ is the nonlinear refractive index, $I_0 = 2\varepsilon_0 c n_0 |A_0|^2$ is the initial peak intensity.

The simulated spectra of amplified pulses and the corresponding spectra of the experimentally measured pulses are shown in figure 4. First of all, it can be seen that the spectral widths in all calculated cases correspond very well to the experimentally measured ones. The discrepancy is only visible for small chirp pulses (shorter than 2 ps), i.e. when strong nonlinear self-modulation occurs. Even in these cases, the spectral profile correlates reasonably well with the experiment. Taking this into account, this model was used for further analysis of amplified pulse compression.

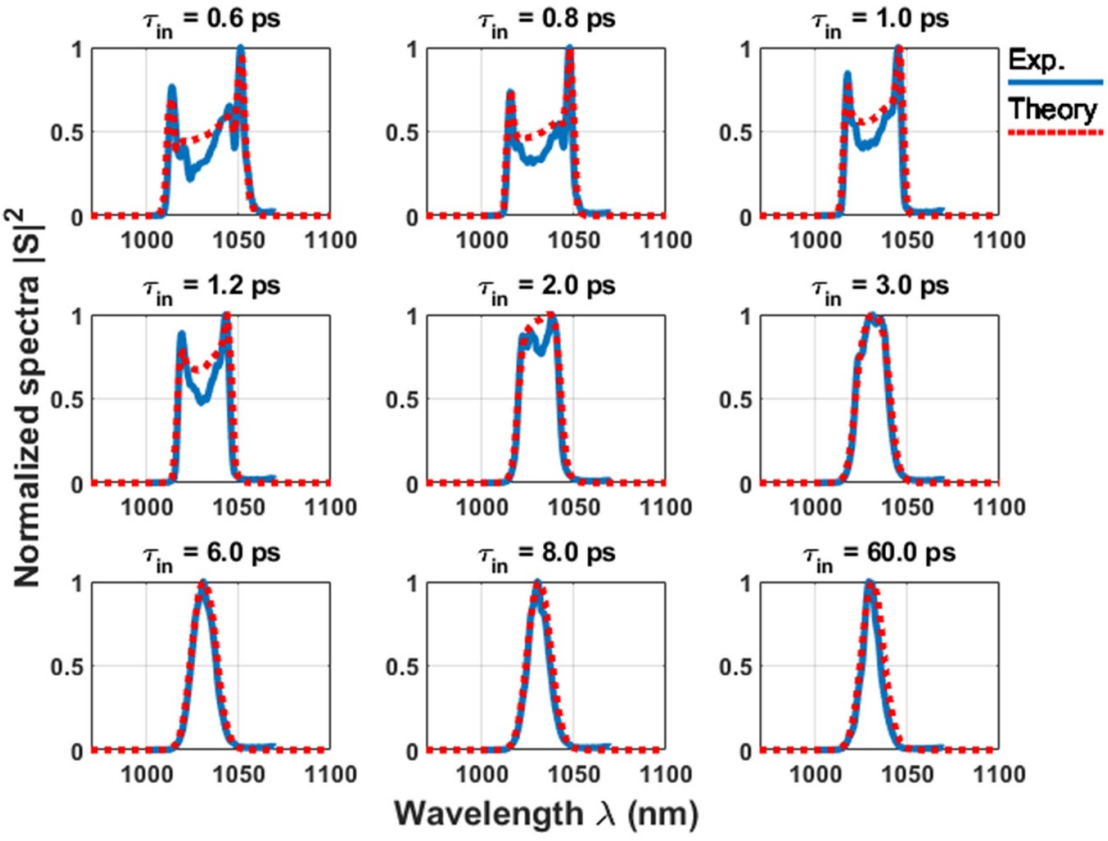

Figure 4. Comparison of simulated (red dotted line) and experimentally measured (blue solid line) spectra of the amplified pulse by varying the chirp of the initial pulse. Model parameters $\tau_\mathrm{K} = 5$ fs, $\tau_\mathrm{G} = -16$ fs, initial signal average power $P_{\mathrm{s,in}} = 5.4$ W, initial pulse duration $\tau_\mathrm{in} = \tau_{1/2}\sqrt{1+\gamma^2}$, $\tau_{1/2} = 100$ fs (FWHM), chirp $5.9 \leqslant \gamma \leqslant 600$.

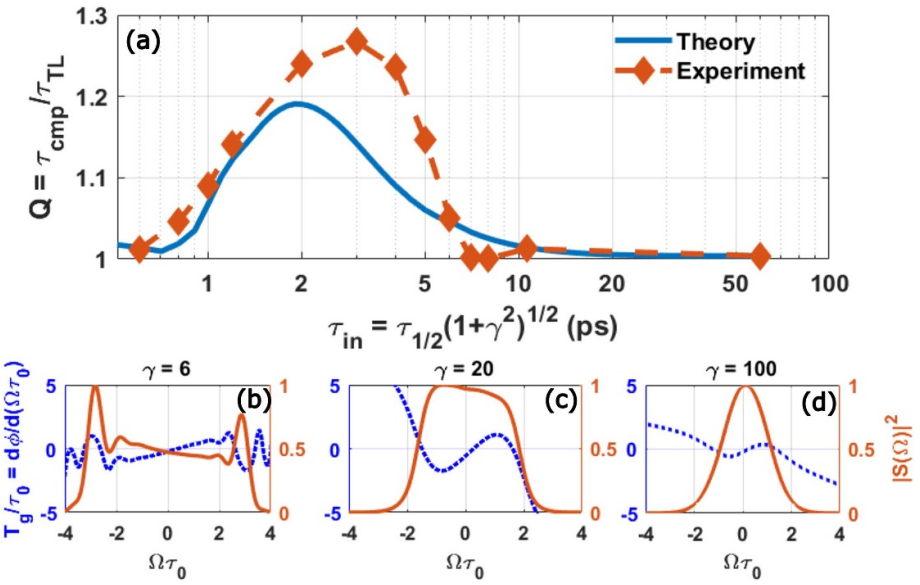

Figure 5. (a)—The ratio of compressed and transform-limited pulse durations vs initial pulse duration (chirp). Logarithmic scale is used on the x-axis, $\tau_{1/2} = 100$ fs. (b), (c), (d)—Amplified pulse spectra (orange) and group delay (blue) after compression with different chirp values of $\gamma = 6$, $\gamma = 20$ and $\gamma = 100$, respectively.

3.6. Amplified pulse compression analysis

The duration of the compressed pulse is calculated by modifying the spectral phase of the amplified pulse. If the spectral complex amplitude of the amplified pulse is $S(\Omega) = B(\Omega)e^{i\varphi(\Omega)}$, then the complex amplitude of the compressed pulse is

$$A_{\text{cmp}}t) = \int_{-\infty}^{\infty} B(\omega)\, e^{i(\varphi(\Omega) - q\Omega^2/2) + i\Omega t}\, \frac{d\Omega}{2\pi}. \tag{36}$$

The optimal compression parameter q is found numerically by searching for when the pulse duration τ_{cmp} (FWHM) becomes the smallest. The quality of pulse compression is characterized by the ratio $Q = \tau_{\text{cmp}}/\tau_{\text{TL}}$, where τ_{TL} is the pulse duration of the TL pulse (FWHM). From the definition it follows that in the case of ideal compression $Q = 1$ and $Q > 1$ otherwise. The numerically calculated and experimentally measured ratio Q at different initial pulse chirps is shown in figure 5(a). Although there is no exact match, it can be seen that both the numerically calculated and experimentally measured parameters Q depend similarly on the initial pulse chirp γ. The discrepancy can be easily explained by the fact that in an experiment, the optical elements always have some aberrations and are likely not ideally positioned. Moreover, in numerical simulation, pulse compression is achieved by modifying only the second-order spectral phase of the pulse, while in a real experiment, the higher-order spectral phase coefficients are also modified. Nevertheless, the results clearly show that if the initial pulse chirp is not properly chosen, the amplified pulse will not be compressed to a TL pulse, regardless of how well the pulse compressor is set up. The physical origin of poor pulse compressibility can be explained through normalized group delay T_g/τ_0 shown in figure 5(b)–(d). At low ($\gamma = 6$) and high ($\gamma = 100$) chirp values, the group delay variation within the spectrum profile remains relatively small, approximately ± 1. This corresponds to an almost linear group delay across the main spectral lobe, which remained after compensating quadratic dispersion. As a result, these conditions lead to good pulse compressibility. In contrast, for the intermediate chirp ($\gamma = 20$) the group delay exhibits strong, highly nonlinear curvature, with magnitude varying from 1 to > -5, precisely within the spectral region that carries most of the pulse energy. Higher frequency components accumulate disproportionately larger delay than lower frequency components, producing a distorted spectral phase that contains significant higher order dispersion components. Such phase cannot be removed by a second-order compressor, thus leading to the observed maximum value of the compression factor Q. The complex interplay between material dispersion and nonlinear SPM during pulse amplification, generates a complicated group delay profile that a simple quadratic compressor cannot remove. It is important to note, that the interval of initial pulse chirp depends on the initial seed and amplified signal power. Using the previously described model, we evaluated how the compression quality Q and output power $P_{\text{s,out}}$ of the amplified pulse change depending on the initial seed pulse chirp, its power and the pump beam power (figure 6). Although the range

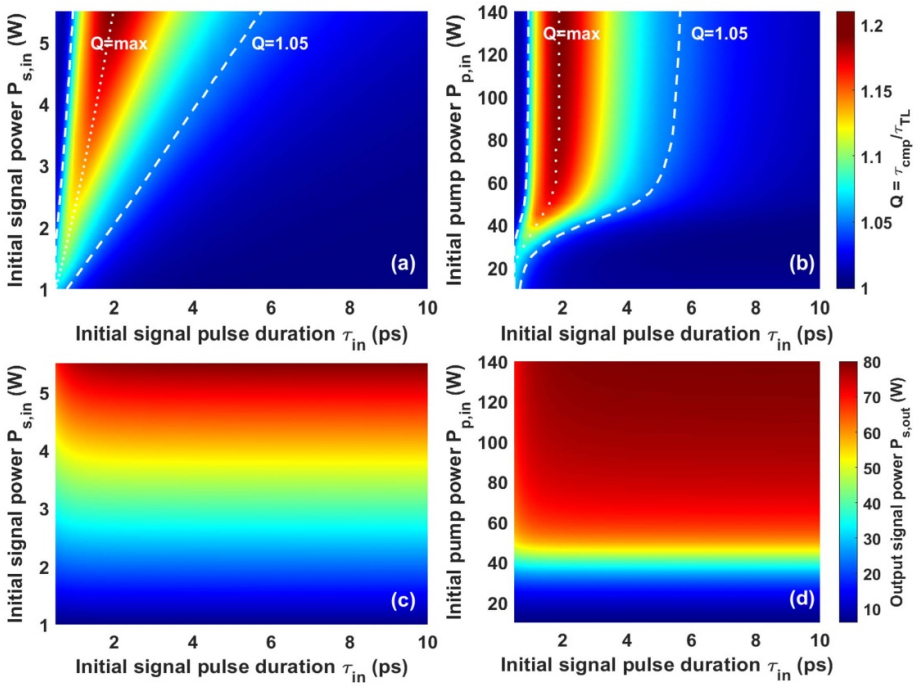

Figure 6. (a)—Calculated compression quality Q and (c) output power $P_{s,out}$ of amplified signal pulse vs initial pulse duration and signal input power when pump power is $P_{p,in} = 140$ W. (b)—The compression quality Q and (d) output power $P_{s,out}$ of amplified signal pulse vs initial signal pulse duration and pump input power when signal initial power is $P_{s,in} = 5.4$ W.

of inappropriate chirp values depends on the chosen tolerable level Q (we use $Q = 1.05$), the simulation results show that for maximum power used in the experiment $P_{p,in} = 140$ W, the range of inappropriate chirp values expands almost linearly with increasing initial signal power (figure 6(a)). Meanwhile, the output power is practically independent of the initial pulse chirp and grows approximately linearly with increasing initial pulse power (figure 6(c)). On the other hand, when the initial signal pulse power is fixed (we use the experimental value $P_{s,in} = 5.4$ W), then as the gain increases, the range of inappropriate chirp values initially increases rapidly, but after exceeding a certain pump beam power it stabilizes and changes very little (figure 6(b)). As before, the average power of the amplified pulse does not depend on the value of its initial chirp (figure 6(d)).

Tendencies described in figures 5 and 6 be can categorized into three main distinct regimes: low initial pulse chirp (<1 ps), intermediate chirp (1–10 ps) and high initial pulse chirp (>10 ps). In case of low pulse pre-chirp (<1 ps), the pulse exhibits high peak intensity, resulting in strong SPM-induced nonlinear phase modulation. The nonlinear phase leads to a significant modulation of the instantaneous frequency. Due to SPM, the leading edge of the pulse experiences a negative instantaneous frequency shift, while the trailing edge acquires a positive frequency shift. Since SPM occurs from the very beginning of the fiber and its material exhibits positive GVD in this spectral range, the fiber acts as a pulse compressor and compensates the SPM-induced frequency modulation for the negatively chirped spectral components, while further broadening the central part of the pulse. Consequently, the pulse entering the transmission diffraction grating compressor exhibits a nearly linear chirp across its entire spectrum, enabling efficient pulse compression. In case the input pulse is strongly pre-chirped (>10 ps), its peak power is substantially reduced and thus the accumulated nonlinear spectral phase shift in the fiber amplifier remains small. Consequently, the contribution of SPM to the pulse dynamics during amplification is negligible. In this regime the spectral phase of the pulse propagating through the fiber is primarily determined by the diffraction grating stretcher. Therefore, the compressor can fully reverse this linear chirp, leading to effective pulse recompression. Lastly, in our opinion, in the intermediate regime (1–10 ps), the initial intensity is insufficient to induce significant SPM at the fiber input. However, as the pulse propagates and is amplified, its peak intensity gradually increases, enhancing the nonlinear phase accumulation. The resulting instantaneous frequency modulation becomes significant near the fiber output, where the local SPM-induced chirp is strong. Since this SPM-induced negative chirp is asymmetric, it is not balanced by the fiber material's positive GVD, the diffraction grating compressor cannot fully compensate the accumulated nonlinear phase, resulting in degraded pulse compressibility and residual temporal pedestals.

4. Conclusions

In conclusion, we have presented a theoretical investigation of pulse amplification and compression in a hybrid PCMA-FCPA laser system supported by experimentally obtained results. The system is seeded with a commercial Kerr-lens mode-locked Yb:KGW oscillator, which drives pulse amplification in a diode-pumped, Yb-doped, polarization-maintaining, double-clad, rod-type LMA PCF. The variation of pulse duration was achieved by implementing a transmission diffraction gratings-based pulse stretcher and compressor. The developed numerical model, which includes interplay between gain dynamics, dispersion and nonlinear SPM, shows excellent agreement with experimental results. Both the simulations and measurements reveal that the initial pulse chirp plays a critical role in determining the quality of pulse compression. In particular, an improper choice of input chirp can lead to incomplete pulse compression regardless of how well the pulse compressor is set up, while maintaining the amplified output power. These results provide valuable guidance for the design and optimization of high average power, high repetition rate femtosecond laser systems capable of delivering nearly TL pulses, which could be used for the development of wavelength-tunable sources, such as optical parametric amplifiers or optical parametric oscillators, for applications in metrology [32], spectroscopy [33] and microscopy [34].

Acknowledgments

This work has received funding from the Research Council of Lithuania (LMTLT), grant S-MIP-23-23.

Data availability statement

All data that support the findings of this study are included within the article (and any supplementary files).

Author contributions

Jokūbas Pimpė 0009-0000-5138-3759
Conceptualization (equal), Data curation (equal), Formal analysis (equal), Investigation (equal), Validation (equal), Writing – original draft (equal), Writing – review & editing (equal)

Vygandas Jarutis 0009-0000-3700-7220
Data curation (equal), Formal analysis (equal), Methodology (equal), Software (equal), Writing – original draft (equal), Writing – review & editing (equal)

Julius Vengelis 0000-0001-8387-1212
Conceptualization (equal), Funding acquisition (equal), Methodology (equal), Resources (equal), Supervision (equal), Writing – original draft (equal), Writing – review & editing (equal)

References

[1] Lv Z, Teng H, Wang L, Wang R, Wang J and Wei Z 2016 High power mode-locked rod-type fiber femtosecond laser with microjoule energy *Opt. Commun.* **370** 156–9
[2] Velsink M C, Illienko M, Chaudhary K and Witte S 2025 Improving signal-to-noise ratios in pump-probe spectroscopy on light-sensitive samples by adapting pulse repetition rates *Opt. Express* **33** 23632–44
[3] Fermann M E and Hartl I 2013 Ultrafast fibre lasers *Nat. Photon.* **7** 868–74
[4] Manchee C, Möller J and Miller R 2019 Highly stable, 100 W average power from fiber-based ultrafast laser system at 1030 nm based on single-pass photonic-crystal rod amplifier *Opt. Commun.* **437** 6–10
[5] Skliutas E, Merkininkaitė G, Maruo S, Zhang W, Chen W, Deng W, Greer J, von Freymann G and Malinauskas M 2025 Multiphoton 3D lithography *Nat. Rev. Methods Primers* **5** 15
[6] Orthaus S, König M, Schönau T, Buschmann V, Tannert S, Lauritsen C, Koberling F, Ortmann U and Erdmann R 2013 Crossing the limit towards deep UV *Opt. Photonik* **8** 33–36
[7] Pupeza I *et al* 2013 Compact high-repetition-rate source of coherent 100 eV radiation *Nat. Photon.* **7** 608–12
[8] Saraceno C J *et al* 2012 Sub-100 femtosecond pulses from a SESAM mode-locked thin disk laser *Appl. Phys.* B **106** 559–62
[9] Zhao J, Li W, Wang C, Liu Y and Zeng H 2014 Pre-chirping management of a self-similar Yb-fiber amplifier towards 80 W average power with sub-40 fs pulse generation *Opt. Express* **22** 32214–9
[10] Lv Z, Yang Z, Li Q, Li F, Wang Y, Zhao W and Yang X 2020 Photonic crystal rod-based high-performance ultrafast fiber laser system *High Power Laser Sci. Eng.* **8** e40
[11] Deslandes P, Perrin M, Saby J, Sangla D, Salin F and Freysz E 2013 Picosecond to femtosecond pulses from high power self mode-locked ytterbium rod-type fiber laser *Opt. Express* **21** 10731–8
[12] Zhao Z, Sheehy B and Minty M 2017 Generation of 180 W average green power from a frequency-doubled picosecond rod fiber amplifier *Opt. Express* **25** 8138–43
[13] Pedersen M E, Johansen M M, Olesen A S, Michieletto M, Gaponenko M and Maack M D 2022 175 W average power from a single-core rod fiber-based chirped pulse amplification system *Opt. Lett.* **47** 5172–5

[14] Jauregui C, Stihler C and Limpert J 2020 Transverse mode instability *Adv. Opt. Photon.* **12** 429–84
[15] Li H, Bu X, Shi Y, Peng Z, Xu Y, Cheng Z and Wang P 2020 High-power chirped pulse amplification based on Yb-doped rod-type PCF and nonlinear amplifying loop mirror oscillator *Proc SPIE* **11437** 194–9
[16] Limpert J *et al* 2005 High-power rod-type photonic crystal fiber laser *Opt. Express* **13** 1055–8
[17] Liu D, Mao X, Bi G, Li T, Zang D and Sun N 2023 Efficiency enhancing technique for rod fiber picosecond amplifiers with optimal mode field matching *Micromachines* **14** 450
[18] Zhao W, Hu X and Wang Y 2014 Femtosecond-pulse fiber based amplification techniques and their applications *IEEE J. Sel. Top. Quantum Electron.* **20** 512–24
[19] Liu W, Schimpf D N, Eidam T, Limpert J, Tünnermann A, Kärtner F X and Chang G 2015 Pre-chirp managed nonlinear amplification in fibers delivering 100 W, 60 fs pulses *Opt. Lett.* **40** 151–4
[20] Ruehl A, Marcinkevicius A, Fermann M E and Hartl I 2010 80 W, 120 fs Yb-fiber frequency comb *Opt. Lett.* **35** 3015–7
[21] Limpert J, Schreiber T, Clausnitzer T, Zöllner K, Fuchs H-J, Kley E-B, Zellmer H and Tünnermann A 2002 High-power femtosecond Yb-doped fiber amplifier *Opt. Express* **10** 628–38
[22] Liu Y, Li W, Luo D, Bai D, Wang C and Zeng H 2016 Generation of 33 fs 93.5 W average power pulses from a third-order dispersion managed self-similar fiber amplifier *Opt. Express* **24** 10939–45
[23] Zhang Y *et al* 2020 High-power pre-chirp managed amplification of circularly polarized pulses using high-dispersion chirped mirrors as a compressor *OSA Contin.* **3** 1988–98
[24] Banys J and Vengelis J 2022 Efficient single-pass and double-pass pre-chirp managed Yb-doped rod-type fiber amplifiers using Gires-Tournois interferometric mirrors *Optik* **249** 168185
[25] Sidorenko P, Fu W and Wise F 2019 Nonlinear ultrafast fiber amplifiers beyond the gain-narrowing limit *Optica* **6** 1328–33
[26] Hua Y, Chang G, Kärtner F X and Schimpf D N 2018 Pre-chirp managed, core-pumped nonlinear PM fiber amplifier delivering sub-100-fs and high-energy (10 nJ) pulses with low noise *Opt. Express* **26** 6427–38
[27] Chen H-W, Lim J, Huang S-W, Schimpf D N, Kärtner F X and Chang G 2012 Optimization of femtosecond Yb-doped fiber amplifiers for high-quality pulse compression *Opt. Express* **20** 28672–82
[28] Eidam T, Hadrich S, Roser F, Seise E, Gottschall T, Rothhardt J, Schreiber T, Limpert J and Tünnermann A 2009 A 325-W-average-power fiber CPA system delivering sub-400 fs pulses *IEEE J. Sel. Top. Quantum Electron.* **15** 187–90
[29] Pimpė J, Banys J, Armalytė S, Neto J J, Jarutis V, Dubietis A, Vengelis J and Stable H 2025 72 W average power, 76 MHz repetition rate femtosecond hybrid PCMA-FCPA Yb-fiber amplifier *Opt. Laser Technol.* **190** 113261
[30] Wang Y, Liu Y, Zhang Z and Kaertner F 2021 Amplification of 1.08 GHz repetition rate femtosecond laser pulses to 97 W average power by a fiber amplifier *OSA Contin.* **4** 1571–6
[31] Paschotta R, Nilsson J, Tropper A C and Hanna D C 1997 Ytterbium-doped fiber amplifiers *IEEE J. Quantum Electron.* **33** 1049–56
[32] Pecile V F, Leskowschek M, Modsching N, Wittwer V J, Südmeyer T and Heckl O H 2024 Record-high power, low phase noise synchronously-pumped optical parametric oscillator tunable from 2.7 to 4.7 μm *Appl. Phys. Lett.* **125** 231108
[33] Shumakova V and Heckl O 2024 A short guide to recent developments in laser-based gas phase spectroscopy, applications and tools *APL Photonics* **9** 010803
[34] Zhao H, Cisek R, Karunendiran A, Tokarz D, Stewart B A and Barzda V 2019 Live imaging of contracting muscles with wide-field second harmonic generation microscopy using a high power laser *Biomed. Opt. Express* **10** 5130–5